
Self-assembly of a binary mixture of particles and diblock copolymers

Jae Youn Lee,^a Russell B. Thompson,^{†a} David Jasnow^b and Anna C. Balazs^{*a}

^a Department of Chemical and Petroleum Engineering, University of Pittsburgh, Pittsburgh PA 15261, USA

^b Department of Physics and Astronomy, University of Pittsburgh, Pittsburgh, PA 15261, USA

Received 23rd May 2002, Accepted 7th June 2002

First published as an Advance Article on the web 7th October 2002

Using theoretical models, we undertake the first investigation into the synergy and rich phase behavior that emerges when binary particle mixtures are blended with microphase-separating copolymers. We isolate an example of spontaneous hierarchical self-assembly in such hybrid materials, where the system exhibits both nanoscopic ordering of the particles and macroscopic phase transformation in the copolymer matrix. Furthermore, the self-assembly is driven by entropic effects involving all the different components. The results reveal that entropy can be exploited to create highly ordered nanocomposites with potentially unique electronic and photonic properties.

Introduction

The combination of organic polymers and inorganic particles can lead to a composite material that is more useful than either of the individual components. By carefully picking the particles and polymers, designers can tailor composites to meet the final product requirements that could not be achieved using other materials. The formation of *nanostructured* composites is a key step in overcoming the obstacles to miniaturization as feature sizes in devices reach the nanoscale. The most efficient route for creating such complex composites is through self-assembly, where cooperative effects among the different components drive the system to form nanostructured materials. Consequently, a particularly important scientific and technological challenge is isolating new routes for promoting the self-assembly between organic polymers and inorganic nanoparticles.

In order to establish these routes, we can exploit the following properties of hard particle mixtures and block copolymer melts. Driven by entropic interactions, binary mixtures of hard, spherical particles that differ only in size have been shown to form a rich variety of structures.¹ For example, a lattice of small spheres can interpenetrate a lattice of large spheres to form a simple cubic, body-centered or face-centered structure.² Driven by similar entropic effects, binary mixtures of particles that differ in shape can also self-organize. In particular, mixtures of nanoscopic spheres and rods can self-assemble into a startling array of ordered structures.³ Driven by enthalpic effects,

[†] Present address: Theoretical Division, Los Alamos National Laboratory, Los Alamos, NM 87545, USA.

block copolymers can microphase-separate into spatially periodic lamellar, cylindrical, spherical or more complicated mesophases.⁴

In this paper, we use theoretical modeling to show that the blending of separately self-organizing particles and block copolymers can be exploited to create novel self-assembled nanostructured materials. In particular, we focus on a small volume fraction of bidisperse spheres in AB diblocks. We show that the introduction of particle bidispersity provides a means of controlling both the morphology of the polymer matrix and the spatial organization of the spheres. Through these studies, we isolate a specific system that simultaneously exhibits the self-assembly of the particles and transformation in the microstructure of the copolymer matrix, creating in a single process a hierarchically structured nanocomposite with potentially unique opto-electronic properties. Furthermore, these morphological changes are driven by entropic effects involving all of the species.

To capture the subtle interplay between the different components in this complex mixture, we employ two distinct theoretical approaches. We first adapt our recently developed approach that combines a self-consistent field theory (SCFT) for the chains and a density functional theory (DFT) for the solid particles.^{5,6} The SCFT has been remarkably successful in describing the thermodynamics of pure polymer systems,⁷ whereas DFTs capture particle ordering and phase behavior in colloidal systems.^{8,9} Applied to a blend of diblocks and *monodisperse* spherical nanoparticles, our integrated SCF/DFT technique identified new self-assembled morphologies, where both particles and polymers form spatially periodic mesostructures.^{5,6} A powerful feature of this method is that we make no *a priori* assumptions about the morphology of the system or the distribution of particles within the different domains. Here, we alter the model to allow for bidispersity in the size distribution of the spheres. To complement the findings from this SCF/DFT approach, we also adapt a scaling theory for particle/diblock mixtures.¹⁰ The scaling theory allows us to readily calculate phase diagrams for the mixture as a function of the ratio of particle sizes and composition of the diblocks.

Below, we provide a brief description of the models we used to probe the behavior of the binary particle/diblock mixtures and then, describe the unique structural organization within these nanocomposites.

The models

The diblock/binary particle mixture consists of a volume fraction ϕ_{p1} of solid spherical particles of radius R_1 and a volume fraction ϕ_{p2} of particles of radius R_2 . Here, $R_1 > R_2$. The mixture also contains a volume fraction $(1 - \phi_p)$ of diblock copolymers, where $\phi_p = \phi_{p1} + \phi_{p2}$, and each copolymer consists of N segments. To characterize the diblocks in our mixture, we let f denote the fraction of A segments per chain. The enthalpic interaction between an A segment and a B segment is described by the dimensionless Flory–Huggins parameter, χ_{AB} . Both the larger (referred to as p_1) and smaller (p_2) spheres are preferentially wetted by the A blocks. That is, the Flory–Huggins interaction parameter between the particles and A is taken as $\chi_{p1A} = \chi_{p2A} = 0$, and the interaction parameter between the different particles and the B species is set equal to χ_{AB} ($\chi_{AB} = \chi_{p1B} = \chi_{p2B} \equiv \chi$). Finally, we note that the nanoparticles are assumed to be comparable in size to the copolymers, and this correspondence of scales plays an important role in the behavior of the system.

To calculate the morphology of the mixture (shown, for example, in Figs. 1–3), we used an extension of SCF/DFT theory.^{5,6} In SCF theory, pair-wise interactions between differing segments are replaced by the interaction of each segment with the average field created by the other segments. Here, we let $w_A(\mathbf{r})$ denote the value at a point \mathbf{r} of the mean field felt by the A segments, $w_B(\mathbf{r})$ denote the field for B segments, and $w_{pi}(\mathbf{r})$ represent the field for the particles, where $i = 1, 2$. Using this approach, the free energy for our system is given by: $F_T = F_e + F_d + F_p$. (The “free energy” discussed here is actually a dimensionless free energy density: $F \rightarrow NF/\rho_0 k_B T V$, where ρ_0^{-1} is a segment volume, k_B is the Boltzmann constant, T is the absolute temperature and V is the volume of the system.) The first term, F_e , details the enthalpic interactions:

$$F_e = (1/V) \int d\mathbf{r} \{ \chi N [\phi_A(\mathbf{r})\phi_B(\mathbf{r}) + \phi_B(\mathbf{r})\phi_{p1}(\mathbf{r}) + \phi_B(\mathbf{r})\phi_{p2}(\mathbf{r})] \} \quad (1)$$

where $\varphi_A(\mathbf{r})$, $\varphi_B(\mathbf{r})$ and $\varphi_{p_i}(\mathbf{r})$ are the local concentrations of A segments, B segments, and the particles, respectively. The diblock entropic free energy F_d is:

$$F_d = (1 - \phi_{p1} - \phi_{p2}) \ln[V(1 - \phi_{p1} - \phi_{p2})/Q_d] - (1/V) \int d\mathbf{r} [w_A(\mathbf{r})\varphi_A(\mathbf{r}) + w_B(\mathbf{r})\varphi_B(\mathbf{r})] \quad (2)$$

where Q_d is the partition function of a single diblock subject to the fields $w_A(\mathbf{r})$ and $w_B(\mathbf{r})$. Finally, the particle entropic contributions to the free energy are given by

$$\begin{aligned} F_p = & (\phi_{p1}/\alpha_{p1}) \ln(V\phi_{p1}/Q_{p1}\alpha_{p1}) + (\phi_{p2}/\alpha_{p2}) \ln(V\phi_{p2}/Q_{p2}\alpha_{p2}) \\ & - (1/V) \int d\mathbf{r} \{w_{p1}(\mathbf{r})\rho_{p1}(\mathbf{r}) + w_{p2}(\mathbf{r})\rho_{p2}(\mathbf{r})\} + \\ & + (1/V) \int d\mathbf{r} \rho_{p1}(\mathbf{r}) \Psi[\bar{\varphi}_{p1}(\mathbf{r}), x_1, x_2] + \rho_{p2}(\mathbf{r}) \Psi[\bar{\varphi}_{p2}(\mathbf{r}), x_1, x_2] \end{aligned} \quad (3)$$

where Q_{p_i} is the partition function of a single particle p_i subject to the field $w_{p_i}(\mathbf{r})$. x_1 and x_2 are the mole fractions of the p_1 and p_2 particles, respectively. The functions $\rho_{p1}(\mathbf{r})$ and $\rho_{p2}(\mathbf{r})$ are the distributions of the centers of the spheres; these functions are dimensionless. The local particle volume fraction $\varphi_{p_i}(\mathbf{r})$ is related to $\rho_{p_i}(\mathbf{r})$ by

$$\varphi_{p_i}(\mathbf{r}) = (4\alpha_{p_i}/(3\pi R_i^3)) \int_{|r'| < R_i} d\mathbf{r}' \rho_{p_i}(\mathbf{r} + \mathbf{r}') \quad (4)$$

The parameter $\alpha_{p_i} = (4\pi R_i^3 \rho_0)/(3N)$ denotes the particle-to-diblock volume ratio, where the R_i are in units of R_0 , the root-mean-square end-to-end distance of the chain. The last two terms in F_p are DFT terms using the expression of Denton and Ashcroft.² They account for the steric interactions between the particles. Ψ is the excess free energy per particle, derived from the Mansoori *et al.* equation of state.¹¹ “Smoothed” densities $\bar{\varphi}_{p1}$ and $\bar{\varphi}_{p2}$ are introduced in the last two terms of eqn. (4) using the Tarazona weighted density approximation.⁸

In the SCFT, $w_A(\mathbf{r})$, $w_B(\mathbf{r})$ and $w_{p_i}(\mathbf{r})$ are determined by locating saddle points in the free energy functional F subject to the incompressibility constraint: $\varphi_A(\mathbf{r}) + \varphi_B(\mathbf{r}) + \varphi_{p1}(\mathbf{r}) + \varphi_{p2}(\mathbf{r}) = 1$. This yields a system of equations that is solved numerically and self-consistently to give possible equilibrium solutions. To obtain these solutions, we implement the “combinatorial screening technique” of Drolet and Fredrickson.¹² We make an initial random guess for the fields and calculate all the densities and the free energy at each step; the fields are then recalculated and the entire process is repeated until changes in the diblock densities at each step become sufficiently small. In addition, we also minimize our free energy with respect to the size of the simulation box, as proposed by Bohbot-Raviv and Wang.¹³

To demonstrate the generality of our predictions, we also use a strong segregation scaling theory¹⁰ (Figs. 3 and 4). The chains are assumed to be highly stretched; the melt is divided into pure-A and pure-B domains, separated by narrowed interfacial regions.¹⁴ The balance between the stretching free energy of the blocks and the energy of the A–B interfaces determines the equilibrium morphology of the pure diblock melt. As above, we introduce a volume fraction ϕ_p of A-like particles, of which ϕ_{p1} are the larger particles and ϕ_{p2} are the smaller ones. The total volume fraction of diblocks is $\phi_d = (1 - \phi_p)$, where $(f\phi_d)$ is the volume fraction of A segments and $(1 - f)\phi_d$ is the volume fraction of B segments.

Small particles can distribute in a relatively uniform manner over both the A and B domains in order to maximize their translational entropy.¹⁵ On the other hand, larger particles possess less translational entropy and thus tend to localize in the energetically more favorable domain;⁵ furthermore, large particles tend to segregate to the center of the compatible phases.^{5,6} Following these observations, we allow the smaller particles to leak into the B domains, with f_2 denoting the fraction in A and $(1 - f_2)$ in B. For simplicity, the smaller particles are assumed to be uniformly distributed within the A and B regions. The larger particles are restricted to the energetically favorable A domains and the distribution of larger particles within A is allowed to vary from uniform to completely segregated. In the latter case, the larger particles are localized near the center of the A domains.

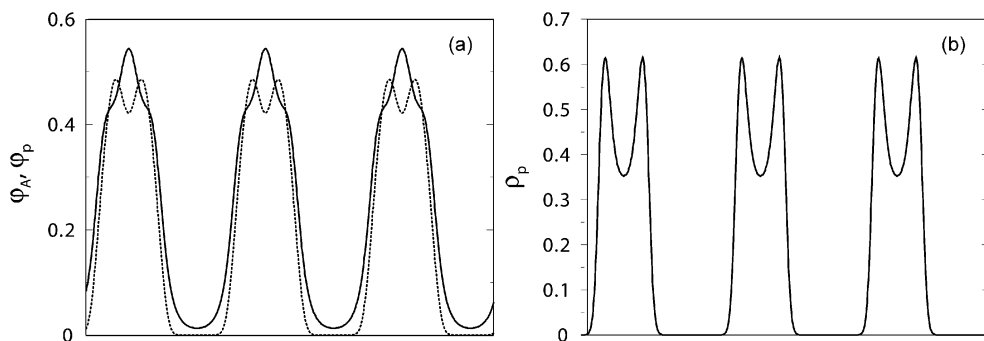


Fig. 1 One-dimensional SCF/DFT density profiles of a *monodisperse* particle/diblock copolymer system. The fraction of A segments per diblock copolymer is $f = 0.30$. The volume fraction of the particles is $\phi_p = 0.20$ and $R_1 = R_2 = 0.2R_0$. (a) The solid curve represents the A block distribution and the dotted curve shows the distribution of particles. (b) The solid curve shows the distribution of the centers of the particles.

The free energy of the ordered structures is:

$$\begin{aligned}
 g_{\text{ordered}} = & (\phi_d/N)\ln\phi_d + (\phi_{p1}/\nu_1)\ln(\psi_{1A}) + (f_2\phi_{p2}/\nu_2)\ln(\psi_{2A}) \\
 & + \left((1-f_2)\phi_{p2}/\nu_2 \right)\ln(\psi_{2B}) + \Psi(\psi_{1A}, \psi_{2A}, n_{1A}, n_{2A},) + n_{2B}\Psi_{\text{CS}}(\psi_{2B}) \\
 & + n_{1A}R_1^2/4Nfa_0^2 + n_{2A}R_2^2/4Nfa_0^2 + n_{2B}R_2^2/(4N(1-f)a_0^2) \\
 & + \chi(1-\psi_{2B})\psi_{2B}(0.5/R_2) + 3\phi_d^{2/3}\chi^{1/3}(2N)^{-2/3}\chi^{2/3}k^{1/3}
 \end{aligned} \quad (5)$$

where ν_i is the volume of a type i sphere, $n_{i\alpha}$ is the number of species i in the α domain and $a_0 = 1/\sqrt{6}$. Here, R_i is in units of a , the segment length, which is set to 1.

The first term describes the translational entropy contribution to the free energy from the diblock copolymers. The following three terms describe the translational entropy contributions from the particles, where $\psi_{i\alpha}$ indicates the local volume fraction of species i in the α domain. The next two terms describe the steric interactions between the particles. The first of the two is the Mansoori *et al.*¹¹ free energy expression for a binary hard sphere mixture, and the latter is the Carnahan–Starling free energy¹⁶ for the smaller particles in the B phase. For $R_1 = R_2$, the Mansoori term Ψ reduces to the Carnahan–Starling expression for monodisperse spheres. The next three terms are associated with the free energy loss due to the stretching of the chains around the particles. The next term describes the Flory–Huggins interaction between smaller particles and B monomers; the term reduces to the expression for diblocks in solvent when $R_2 = 0.5$. The last term is the diblock

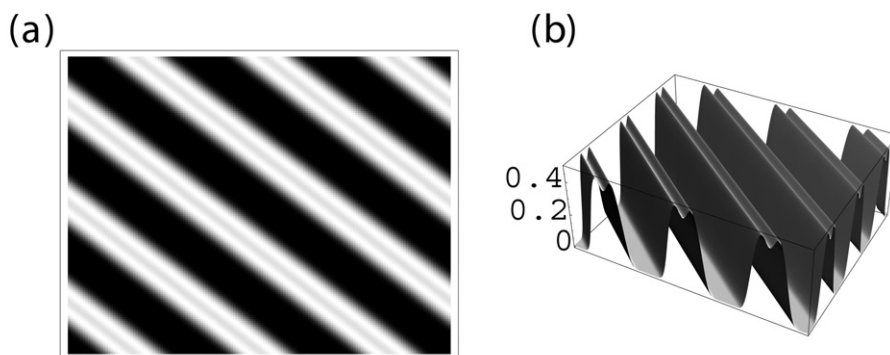


Fig. 2 Two-dimensional SCF/DFT density profiles for the same set of parameters as in Fig. 1. (a) and (b) are density and surface plots, respectively, for the A phase. In (a), the light regions indicate high concentrations of A, while the black regions mark the absence of A. The morphology of the system is clearly lamellar.

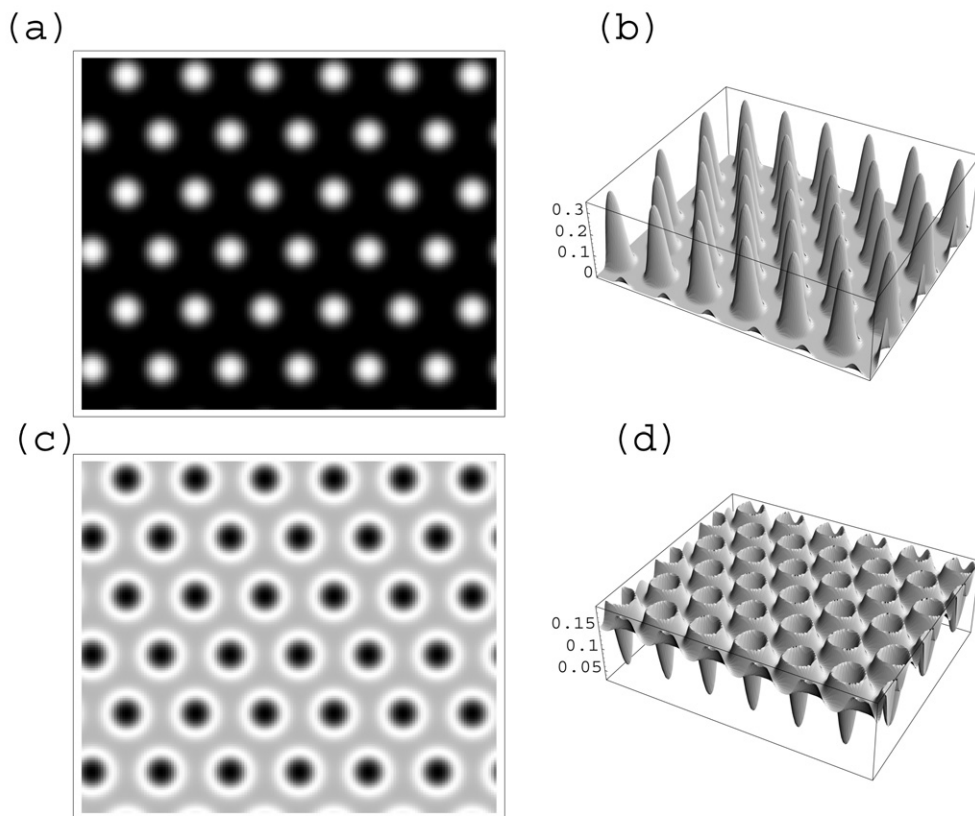


Fig. 3 The bidisperse case is shown in (a)–(d), with the large particle ($\phi_{p1} = 0.05$, $R_1 = 0.2R_0$) density and surface plots shown in (a) and (b), respectively. The small particle ($\phi_{p2} = 0.15$, $R_2 = 0.1R_0$) density and surface plots are displayed in (c) and (d), respectively. As can be seen, a graded cylindrical morphology results from the introduction of the bidispersity.

contribution to the free energy in the strong segregation limit. This term arises from the elastic energy of the chains and the interfacial tension between the different domains.¹⁴ The prefactors λ and κ are both morphology dependent.^{10,14} We only consider the three classical diblock structures: lamellar, cylindrical and spherical.

For each set of parameters for each possible morphology, we minimize eqn. (5) to determine the equilibrium structure. In order to obtain phase diagrams, we compare the free energies of the ordered structures and the disordered phase. In the disordered phase, both particles and diblocks are dispersed uniformly in space. Thus, the free energy for the disordered phase is given by:

$$\begin{aligned}
 g_{\text{disordered}} = & (\phi_d/N)\ln(\phi_d) + (\phi_{p1}/\nu_1)\ln(\phi_{p1}) + (\phi_{p2}/\nu_2)\ln(\phi_{p2}) \\
 & + \Psi(\phi_{p1}, \phi_{p2}, \phi_{p1}/\nu_1, \phi_{p2}/\nu_2) + (\phi_{p1}/\nu_1)R_1^2/4Na_0^2 + (\phi_{p2}/\nu_2)R_2^2/4Na_0^2 \\
 & + \chi(1-f)(1-\phi_p)\phi_{p1}(0.5/R_1) + \chi(1-f)(1-\phi_p)\phi_{p2}(0.5/R_2) \\
 & + \chi f(1-f)(1-\phi_p)^2
 \end{aligned} \quad (6)$$

Results and discussions

In this paper, we are interested in studying binary hard sphere/diblock copolymer mixtures. For the SCF/DFT calculations, the radius of the larger spheres is given by $R_1 = 0.2R_0$, and the radius

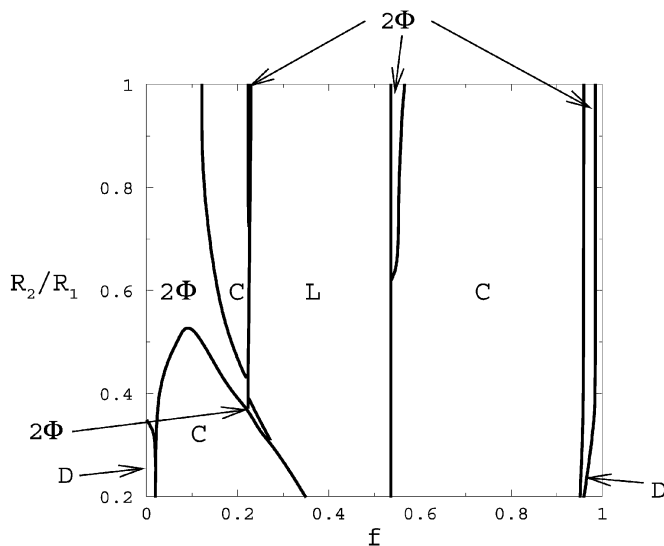


Fig. 4 Phase diagram for mixtures of bidisperse spheres and diblocks calculated using strong segregation theory. R_2/R_1 is the ratio of the smaller to larger particle radii and f is the fraction of A units in the diblock. Letters L and C designate lamellar and cylindrical morphologies, respectively. The regions marked D delineate the location of the disordered phases and the area labeled 2Φ marks the two-phase coexistence region. The total volume fraction of particles is fixed at 20%, of which 3% are the larger and 17% are the smaller spheres. Here, $N = 300$ and $\chi_{p1A} = \chi_{p2A} = 0$, and $\chi_{AB} = \chi_{p1B} = \chi_{p2B} = 1$.

of the smaller spheres is $R_2 = 0.1R_0$. To specify the composition of the diblock, we set $f = 0.3$; that is, each diblock is composed of 30% A monomers and 70% Bs. We fix $\bar{N} = 1000$, where $\bar{N} = \rho_0^2 a^6 N$ is the invariant polymerization index. We also fix $\chi_{AB}N = 20$. As noted above, we focus on the important case of preferential wetting, where $\chi_{p1A} = \chi_{p2A} = 0$ and $\chi_{p1B}N = \chi_{p2B}N = \chi_{AB}N$. This implies that particles of both sizes are completely coated with or are chemically identical to the A species.

As a basis of comparison, we first consider the effect of adding the larger *monodisperse* spheres to the pure diblocks. Here, $R_1 = R_2 = 0.2R_0$. Figs. 1 and 2 show the respective one- and two-dimensional density profiles obtained from the SCF/DFT calculation in the case where 20% of these particles ($\phi_p = 0.20$) are added to the $f = 0.30$ diblock melt. The morphology of the system is clearly lamellar. A close look at Fig. 1(a) reveals a self-assembled morphology where the entire composite displays a spatially periodic structure. We also see that the particles are forced near the A–B interface. This is particularly clear from Fig. 1(b), which shows the particle center distribution. The plots also show that A-block concentration is increased in the center of the A domain.

We now fix f and ϕ_p , but alter the composition of the particle mixture so that there is a 5% volume fraction of larger particles ($\phi_{p1} = 0.05$), with $R_1 = 0.2R_0$, and a 15% volume fraction of smaller particles ($\phi_{p2} = 0.15$), with $R_2 = 0.1R_0$. As a consequence of this change, the system forms a cylindrical mesophase, as shown in Fig. 3(a)–(d). These figures also reveal a new structural feature: the large and small A-like particles are not homogeneously distributed. Now the large particles are concentrated in the center of the domain. In this manner, the A chains do not lose conformational entropy by having to stretch around these large obstacles.⁵ The smaller particles are concentrated near the edge of the A–B interface and, to a large degree, in the incompatible B phase.

Thus, replacing the monodisperse spheres with an equal volume fraction of bidisperse particles has prompted not only a phase transformation in the polymer microstructure but also, the creation of a graded particle film that can typically be tens of nanometres in width. The system constitutes a hierarchically ordered nanocomposite, which has been formed entirely through self-assembly. If the particles were semiconductors, the graded layers could display novel opto-electronic properties,¹⁷

and the filled cylinders can form an array of nanoelectrodes, which can be utilized to fabricate organized nanodevices.¹⁸

A sufficient disparity in particle size is necessary to produce a transition from the lamellar to graded cylindrical phase. This can be seen from the phase diagram shown in Fig. 4, which is shown in the $R_2/R_1 - f$ plane. To obtain this plot, we use the strong segregation scaling theory (SST) for mixtures of diblocks and bidisperse spheres that was described in the Models section. In order for the polymeric system to be in the strong segregation limit, $\chi N \gg 10$. For our calculations, we set $N = 300$ and $\chi = 1$. Since the SST is primarily applicable at low temperatures, we only expect qualitative agreement between the SST and SCF/DFT calculations. Nevertheless, we can focus on the case where $f \approx 0.3$, as in Fig. 3. At $R_2/R_1 = 1$, within the SST, the system forms a lamellar structure similar to the image in Fig. 1(a). However, it is only for $R_2/R_1 \sim < 0.3$, that the mixture forms a cylindrical phase; as shown in Fig. 5, the small particles migrate to the B phase, much as in Fig. 3(a)–(d).

To determine what drives these morphological changes, we can separate the various contributions to the total free energy of the system. Since the SST and SCF/DFT give qualitatively similar results, we present results from the SST analysis. Fig. 5 shows how the contributions to the free energy from the particles vary as a function of R_2/R_1 at $f = 0.28$. The volume fraction of larger particles is fixed at 3%, while the volume fraction of smaller particles is 17%. The inset shows the volume fraction of smaller particles in the A phase ($\phi_{2A} = f_2\phi_{P2}$) and the local volume fraction of larger particles in the A phase (ψ_{1A}) for various R_2/R_1 . The variable ψ_{1A} is a measure of the segregation of the larger particles within the A region; as ψ_{1A} approaches 1, the particles become highly confined in the center of this domain.¹⁰

From the inset, we see that as R_2/R_1 decreases to approximately 0.3, the smaller particles “delocalize” and migrate into the energetically unfavorable B regions. This results in an increase in the enthalpic contribution (see Fig. 5); however, this increase in free energy is offset by the gain in

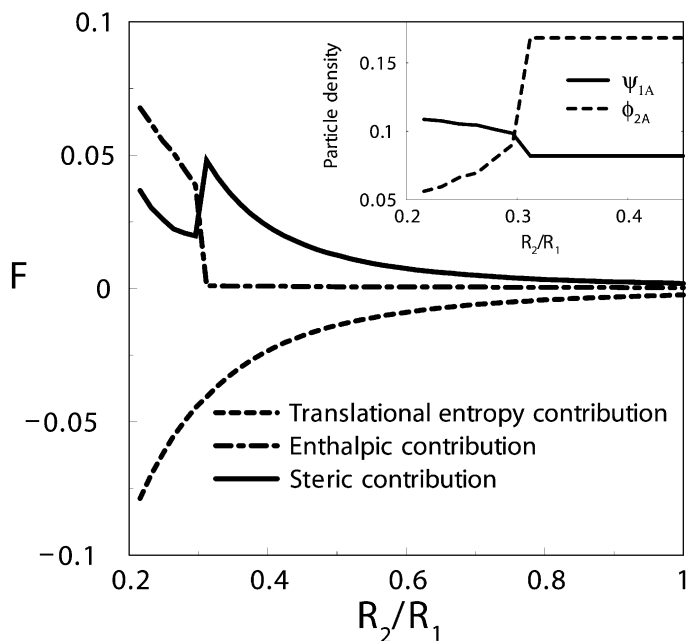


Fig. 5 Decomposition of free energy for bidisperse spheres/diblocks as a function of particle bidispersity calculated using strong segregation theory. Plot is for the same composition of particles as shown in Fig. 4 at $f = 0.28$. The dashed curve is the contribution to the free energy from translational entropy, the dashed/dotted curve is the contribution from the enthalpic interactions and the solid curve indicates the contribution from the steric interactions between particles. The inset shows the fraction of smaller particles in the A phase ($\phi_{2A} = f_2\phi_2$) (dashed curve) and the local volume fraction of larger particles in the A phase (solid curve).

the translational entropy of the smaller particles and a decrease in the steric contribution, which is a measure of the crowding of the hard particles. Apparently, entropy wins, and it is more favorable for the particles to be distributed in the manner shown in Fig. 3(a)–(d) than to have the large and small particles uniformly mixed and confined within the energetically favored A phase.

We also note an increase in ψ_1 at the point where the smaller particles delocalize into B (see inset). In mixtures of small and large particles, there is a “depletion attraction” between the larger objects that is due to the extra volume that is available to the smaller particles when the larger particles approach one another, thus increasing the entropy of the system.^{19,20} Here, we find similar attractions between the larger spheres; in particular, the “enhanced localization” of the larger particles to the central regions of the A blocks coincides with an increase in the translational entropy of the smaller spheres.

There is a significant consequence of the smaller particles migrating to the B phase. In mixtures involving small monodisperse spheres, the migration of these A-like particles into B apparently decreases the effective value of f and thus can drive the system into the cylindrical phase.¹⁷ It is likely that this mechanism is responsible for the transition from lamellar to cylindrical at $f = 0.28$ and $R_2/R_1 \approx 0.3$ in Fig. 4.

We can obtain other novel structures by altering the relative number of smaller and larger particles at fixed ϕ_p and f . We now set $\phi_{p1} = 0.15$ and $\phi_{p2} = 0.05$ at $f = 0.30$. Now, there is a higher volume fraction of larger spheres than smaller particles. This combination of parameters yields a lamellar film of graded nanoparticles within a lamellar matrix, as can be seen in Figs. 6 and 7. Fig. 6(a) is obtained by performing the calculation in one dimension and reveals the 1D density profiles. As can be seen, the larger particles (dashed curve) segregate in the center of the A block (solid curve), while the smaller spheres (dotted curve) are expelled to the edge of the A-phase, and to a large degree into the B domain (B density profiles are not depicted). Again, the particles have microphase-separated into regions of smaller and larger particles. Since all the particles (large and small) are wetted by A and are incompatible with B, there is no enthalpic reason for the small particles to coalesce in the B region. This size-based microphase separation is also apparent by examining the distribution of the centers of the particles as shown in Fig. 6(b). One can see a significant number of small particles (dotted curve) that are separated from the region of large particles (dashed curve). The large-particle region is relatively free of small particles. Fig. 7 shows the result of a two-dimensional calculation on this system; the images show the distribution of the different particles in the lamellar matrix.

The causes for the demixing of the different sized particles in the case shown in Figs. 6 and 7 are similar to reasons cited for the previous case shown in Fig. 3. As the small particles migrate out of the A-phase into the B, the enthalpic contribution to the free energy goes up.²¹ However, this

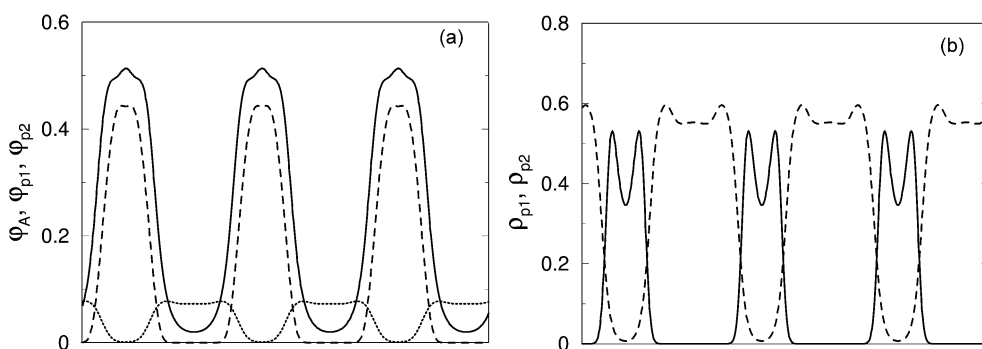


Fig. 6 One-dimensional SCF/DFT density profiles of a bidisperse particle/diblock copolymer system with a fraction of A segments per chain of $f = 0.30$. In (a), the solid curve represents the A block distribution, the dashed curve shows the distribution of the larger $R_1 = 0.2R_0$ particles and the dotted curve shows the smaller $R_2 = 0.1R_0$ particles. The volume fraction of the larger particles is $\phi_{p1} = 0.15$ and the volume fraction of smaller particles is $\phi_{p2} = 0.05$. In (b), the solid curve shows the distribution of the centers of the large particles, while the dashed curve shows the small particle center distribution.

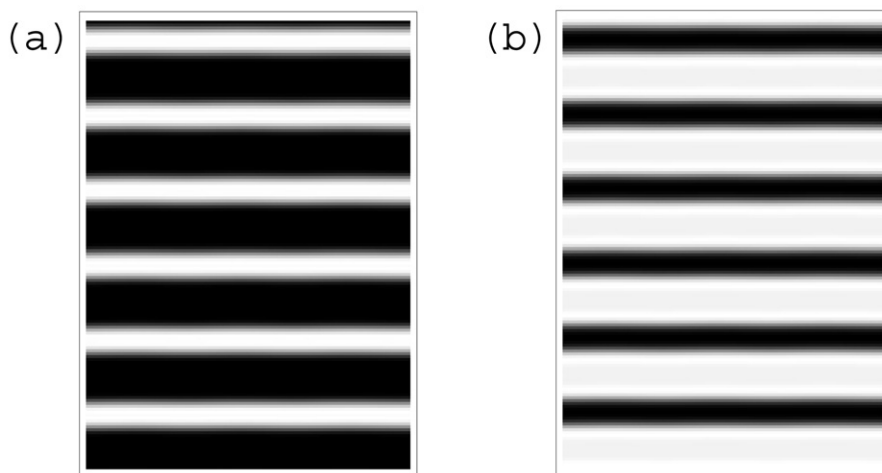


Fig. 7 Two-dimensional SCF/DFT density profiles for the particle distributions for the same parameters as in Fig. 6. (a) Distribution of the larger particles and (b) the smaller particle distribution. The light regions show the presence of a species, whereas the dark regions show the absence of that species.

increase in free energy is more than compensated by two factors: the steric term, and the small-particle translational entropy.²¹ Thus it is entropically more desirable for particles to be segregated in the manner shown in Figs. 6 and 7 than to be relatively mixed and completely localized in the A domain.

Fig. 8 captures and summarizes the rich phase behavior that can be obtained at fixed f and ϕ_p by introducing bidisperse particle mixtures into the copolymer matrix, and by varying the relative composition of the binary particle mixture. In this figure, as in all the examples presented here, $f = 0.3$, $\phi_p = 0.20$ and the particles are preferentially wetted by the A phase. In Fig. 8(a), we see the particle-filled lamellar structure that appears when monodisperse spheres with $R_1 = R_2 = 0.2R_0$ are added to the diblocks. In Fig. 8(b), we show the graded lamellar morphology that can be achieved by introducing bidispersity in particle size with $\phi_{p1} = 0.15$ and $\phi_{p2} = 0.05$. Directly below this image, in Fig. 8(c), is the graded cylindrical phase that results when the relative composition of the binary sphere mixture is shifted to $\phi_{p1} = 0.05$ and $\phi_{p2} = 0.15$. Finally in Fig. 8(d), we show the simple cylindrical structure that appears when smaller monodisperse particles with $R_1 = R_2 = 0.1R_0$ are added to the pure $f = 0.3$ matrix. Thus, not only can one drive a transition from a lamellar to a graded cylinder phase (as discussed in the first part of this paper) but also, a transition from a cylindrical to a graded lamellar phase can be promoted through the introduction of bidisperse particles.

Conclusions

We investigated the self-assembly of binary particle mixtures within a self-organizing medium of diblock copolymers. We focused on the case where the smaller and larger spherical particles are preferentially wetted by the A blocks of the AB diblocks. We found a rich phase behavior where entropic effects give rise to novel nanostructured composites. In particular, a number of entropic effects play a role in the observed transition from the lamellar to graded cylindrical phase. Entropic interactions between the A chains and larger particles, and steric effects between the different particles drive the larger particles to localize near the center of the A domains. In addition, the smaller particles gain translational entropy by delocalizing and migrating into the unfavorable B phase, suggesting a “microphase separation” in the particle system. Here, we isolated a special case where the fraction of smaller particles in the mixture is relatively high and f is sufficiently close to the order–order transition, that the delocalization of these spheres and the lamellar–cylindrical transition in the matrix structure happen simultaneously.

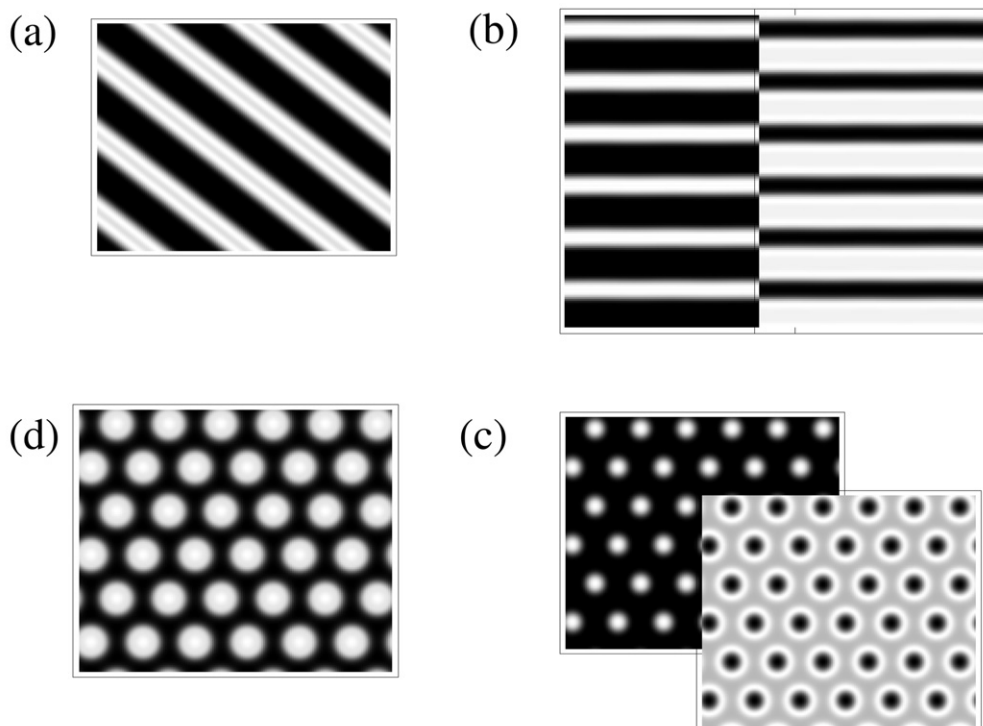


Fig. 8 Two-dimensional SCF/DFT density profiles. Here, $f = 0.3$, $\phi_p = 0.20$ and all the particles are preferentially wetted by the A phase. The figures highlight the variations in morphology that can be achieved by altering the relative size and composition of the particles in the mixture. (a) Particle-filled lamellar structure for $R_1 = R_2 = 0.2R_0$. (b) Graded lamellar morphology that occurs when we introduce particles that are bidisperse in size with $\phi_{p1} = 0.15$ and $\phi_{p2} = 0.05$. (c) Graded cylindrical phase that arises when the composition of the binary particle mixture is shifted to $\phi_{p1} = 0.05$ and $\phi_{p2} = 0.15$. (d) Simple cylindrical structure that appears with smaller, monodisperse particles where $R_1 = R_2 = 0.1R_0$. Thus, by introducing bidispersity in the size of the particles, one can go from (a) to (b) or (c); one can also go from the structure in (d) to (b) or (c).

Other morphologies can be obtained by changing the relative ratio of the smaller to larger particles at fixed values of f and ϕ_p . In particular, we can create a transition from a graded cylindrical structure to a graded lamellar film by altering the values of ϕ_{p1} and ϕ_{p2} . Fig. 6 reveals other transitions that can be obtained by the introduction of bidisperse particles and mixtures and the variation in the relative fraction of each particle species.

We hypothesize that the polydispersity-induced particle microphase separation shown here in the lamellar phase and cylindrical phases will be seen for other diblock morphologies, and thus other graded structures could be fabricated. For example, the same phenomenon should be seen in the spherical morphology, where the large particles would localize in the center of the A spheres and the small particles would form coronas around the larger species.

These findings point to a new methodology for tailoring the particle distributions within the copolymer matrix and/or the overall morphology of the mixture, and thereby controlling the performance of the nanocomposite. The results also reveal that in complex mixtures of hard and soft components, entropy can be exploited to create highly ordered hybrid materials.

Acknowledgements

ACB and DJ thank the NSF and ARO for financial support. ACB also thanks the DOE for financial support.

References

- 1 P. Barlett, R. H. Ottewill and P. N. Pusey, *Phys. Rev. Lett.*, 1992, **68**, 3801 and references therein.
- 2 A. R. Denton and N. W. Ashcroft, *Phys. Rev. A*, 1990, **42**, 7312 and references therein.
- 3 M. Adams, Z. Dogic, S. L. Keller and S. Fraden, *Nature*, 1998, **393**, 349.
- 4 F. Bates and G. Fredrickson, *Phys. Today*, 1999, **52**, 32.
- 5 R. B. Thompson, V. V. Ginzburg, M. W. Matsen and A. C. Balazs, *Science*, 2001, **292**, 2469.
- 6 R. B. Thompson, V. V. Ginzburg, M. W. Matsen and A. C. Balazs, *Macromolecules*, 2002, **35**, 1060.
- 7 M. W. Matsen and F. S. Bates, *Macromolecules*, 1996, **29**, 1091 and references therein.
- 8 P. Tarazona, *Mol. Phys.*, 1984, **52**, 81.
- 9 G. J. Vroege and H. N. W. Lekkerkerker, *Rep. Prog. Phys.*, 1992, **55**, 1241 and references therein.
- 10 J. Huh, V. V. Ginzburg and A. C. Balazs, *Macromolecules*, 2000, **33**, 8085.
- 11 G. A. Mansoori, N. F. Carnahan, K. E. Starling and T. W. Leland, *J. Chem. Phys.*, 1971, **54**, 1523.
- 12 F. Drolet and G. H. Fredrickson, *Phys. Rev. Lett.*, 1999, **83**, 4317.
- 13 Y. Bohbot-Raviv and Z-G. Wang, *Phys. Rev. Lett.*, 2000, **85**, 3428.
- 14 N. Semenov, *Sov. Phys. JETP*, 1985, **61**, 733.
- 15 J. Y. Lee, R. Thompson, D. Jasnow and A. C. Balazs, *Macromolecules*, in press.
- 16 N. F. Carnahan and K. E. Starling, *J. Chem. Phys.*, 1969, **51**, 635.
- 17 N. Kotov, *Mater. Res. Bull.*, 2001, **26**, 992.
- 18 E. Jeoung *et al.*, *Langmuir*, 2001, **17**, 6396.
- 19 A. D. Dinsmore, A. G. Yodh and D. J. Pine, *Phys. Rev. E*, 1995, **52**, 4045.
- 20 A. D. Dinsmore, A. G. Yodh and D. J. Pine, *Nature*, 1996, **383**, 239 and references therein.
- 21 R. B. Thompson, J.-Y. Lee, D. Jasnow and A. C. Balazs, *Phys. Rev. E*, submitted.